ACS OMEGA

http://pubs.acs.org/journal/acsodf

Article

Effect of the Fuel Equivalence Ratio on the Mechanisms of Thiophene Oxidation in Water Vapor at Increased Density of the Reagents

Oxana N. Fedyaeva,* Andrey V. Shishkin, and Anatoly A. Vostrikov

Cite This: *ACS Omega* 2021, 6, 13134−13143

Read Online

ACCESS | Metrics & More | Article Recommendations

ABSTRACT: The article presents the results of a study of thiophene oxidation in high-density C_4H_4S/O_2 mixtures (ρ_{Thi} = 0.12 and 0.15 mol/dm^3, ρ_{O2} = 0.74−1.26 mol/dm^3), diluted with water vapor and argon (dilution level x_D = 35−65% mol), at uniform heating (1 K/min) of a stainless-steel tubular reactor up to 823 K. It is established that the temperature of thiophene oxidation onset weakly depends on the nature of the diluent and the oxygen content in the reaction mixture. From the time dependences of the reaction mixtures on temperature and pressure, it follows that the oxidation of thiophene in the water vapor and argon media proceeds according to the mechanisms of homogeneous and heterogeneous reactions. Upon oxidation of thiophene in the stoichiometric mixtures in argon with a small amount of water vapor, as well as in the lean mixtures in water vapor, the contribution of reactions on the surface of the Pt−Rh/Pt thermocouple, inserted into the center of the reaction volume, is increased. Upon oxidation of thiophene in water vapor in the fuel-enriched and stoichiometric mixtures, reactions on the oxidized surface of the reactor wall (primarily iron oxides) prevail. Increasing the density of water vapor both reduces the contribution of heterogeneous reactions on the reactor wall and prevents complete carbon burnout. It is shown that the neutralization of sulfuric acid, resulting from the oxidation of thiophene, with calcium carbonate reduces the corrosion of stainless steel. The X-ray diffraction analysis revealed the presence of ferrochromite, iron and chromium oxides, iron, nickel, and chromium sulfates in the corrosion products.

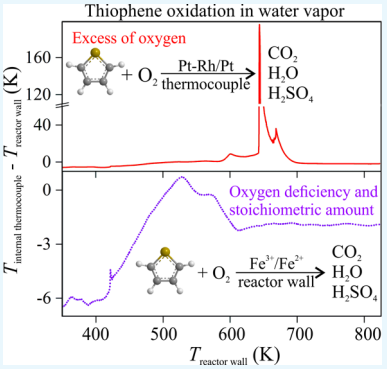

1. INTRODUCTION

Depletion of light oil reserves and increased consumption of motor fuels lead to the involvement in the processing of heavy oil raw materials (heavy oil, bitumen, tar, and oil shale), characterized by a high content of thiophene derivatives.[1−4] The accumulation of waste from the production and processing of such raw materials causes environmental problems, in particular, pollution of nearby water areas.[5,6] Incineration of these wastes by conventional methods leads to the release of SO_2 and aerosol particles (primarily soot) into the atmosphere.[7,8] Since these wastes are usually waterlogged, the use of high-density water vapor or supercritical water (SCW: T > 647 K, P > 22.1 MPa) can become one of the ways of their environmentally safe processing.[9,10] The latter, in particular, is determined by the fact that the final product of oxidation of S-containing organic substances in an aqueous-oxygen mixture is sulfuric acid.[11,12] It is obvious that for the development of new technologies based on the combustion of fuels and wastes in dense water vapor or SCW, it is necessary to obtain data on the oxidation features of the individual compounds in these media. Oxidation of several hydrocarbons and heteroatomic compounds was studied earlier.[13−15] The present research is aimed at identifying the features of thiophene oxidation, as the simplest aromatic S-containing compound, in an aqueous medium.

From the analysis of the literature, it follows that in the absence of oxidants, thiophene derivatives are thermally stable. Winkler *et al.*[16] used GC−MS to study the composition of thiophene pyrolysis products within the temperature range of 773−1373 K. It was established that at T < 1073 K, significant fragmentation of the thiophene skeleton does not occur; only C−H bonds are cleaved, and the resulting thiophenyl radicals recombine to form di- and terthiophenes as condensation products. At T > 1173 K, skeleton fragmentation becomes more intense and the amount of small S-containing products, such as CS_2 and H_2S increases.[16] Katritzky *et al.*[17] showed that at 733 K, thiophene does not transform in SCW for 60 min. Patwardhan *et al.*,[18] when studying the conversion of thiophene in SCW (673 K, 23.5 MPa, reaction time 31 min,

Received: February 19, 2021
Accepted: May 3, 2021
Published: May 11, 2021

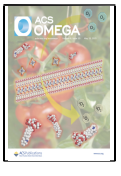

Table 1. Experimental Conditions[a]

test (diluent)	partial pressure (MPa) O_2	partial pressure (MPa) Ar	amount of components (mmol) $n_0(C_4H_4S)$	$n_0(O_2)$	$n_0(CaCO_3)$	$n_0(D)$	φ	x_D (% mol)	P_R (MPa)[c]
1 (Ar + H_2O)	1.87	3.82	7.6	48.6		100.6 (1.7)[b]	1.01	64	4.72
2 (Ar + H_2O)	2.52	3.85	10.1	65.4		100.4 (1.7)[b]	1.01	57	
3 (H_2O)			10.1			50			2.60
4 (H_2O)	1.92		10.1	49.5		50	1.33	46	1.26
5 (H_2O)	2.52		10.1	65.4		50	1.01	40	1.38
6 (H_2O)	3.18		10.1	82.5		50	0.80	35	1.76
7 (H_2O)	3.22		10.1	82.0	20.2	50	0.80	35	1.94
8 (H_2O)	3.17		10.1	80.9		100	0.81	52	1.62

[a]Here $\varphi = 6.5n_0(C_4H_4S)/n_0(O_2)$ is the fuel equivalence ratio according to the stoichiometric coefficients of reaction 1 and x_D (%) = $100n_0(D)/[n_0(D) + n_0(C_4H_4S) + n_0(O_2)]$ is the dilution level of the C_4H_4S/O_2 mixture. [b]Residual amount of water in the heated part of the reactor calculated using the reference data[27] is given in brackets. [c]P_R is the pressure in the reactor after the end of the test at a temperature of 298 K.

autoclave with stirrer, weight ratio $H_2O/C_{16}H_{34}$ = 1:1), found that the degree of its desulfurization (the proportion of sulfur atoms converted into H_2S) did not exceed 3−5%. Qi *et al.*,[19] when studying the conversion of thiophene in SCW (673 K, 23.5 MPa, reaction time 60 min, autoclave with stirrer, weight ratio $H_2O/C_{14}H_{30}$ = 1:1) determined that the degree of desulfurization was equal to 18.8%. According to Timko *et al.*,[20] the SCW conversion of S-containing compounds proceeds *via* the formation of free radicals, while the transfer of the H atom from the neighboring C−H bond to the sulfur atom is a limiting stage. Kang *et al.*,[21] based on the results of thermal decomposition and SCW conversion of hexyl sulfide and hexanethiol (673 K, 24.7−25.6 MPa, reaction time ≤30 min, autoclave) concluded that water can act as a H-transfer catalyst and reactant; in the absence of water, aromatic sulfur compounds such as thiophenes are produced due to the hydrogen deficiency in thermal decomposition.

The results obtained by Khalil *et al.*[22] show that the degree of hydrothermal conversion of thiophene increases with increasing reaction time (≈72 h), temperature (393−553 K), and hematite concentration (≈0.1 wt %) but decreases with increasing thiophene/water ratio (from 3:7 to 7:3). Yoshida *et al.*,[23] when studying the conversion of thiophene in SCW (673 K, 10−60 min exposure time, Hastelloy C-276 alloy autoclave) in the presence of NaOH (1−5 mol/dm^3) and iron powder (≤0.1 mol, 300 mesh), revealed that its complete desulfurization was achieved at the maximum exposure times and the concentration of additives. The authors suggested[23] that in the presence of NaOH, thiophene desulfurization proceeds according to the ionic mechanism, while in the absence of iron powder, the process is catalyzed by the reactor wall.

Based on the large activation barrier (>125.5 kJ/mol) of direct oxidation of thiophene by ground-state oxygen, Song *et al.*[24] concluded that this reaction might be important only in high-temperature processes. In the presence of a catalyst, the activation barrier decreases and a high degree of thiophene conversion can be achieved at moderate temperatures.[25] From the above overview, it follows that the amount of data on the thiophene oxidation in a water−oxygen mixture is severely limited, and the mechanisms for the involvement of water and oxygen in this process are not clearly understood.

The present work aims at identifying the effect of the fuel equivalence ratio and dilution level of the C_4H_4S/O_2 mixture on the mechanisms of thiophene oxidation in water vapor and argon at uniform slow heating in a context of the high density of reagents and the diluent. Since argon is an inert diluent, a comparison of the thiophene oxidation in water vapor and argon will allow revealing the role of H_2O molecules in this process.

2. RESULTS AND DISCUSSION

Taking into account the fact that the final oxidation product of S-containing organic compounds in the water medium is sulfuric acid,[11,12] oxidation of thiophene by oxygen is described by the following gross reaction

$$C_4H_4S^{(g)} + 6.5O_2{}^{(g)} \rightarrow 4CO_2{}^{(g)} + H_2O^{(g)} + H_2SO_4{}^{(g)},$$
$$\Delta_r H^\circ_{298} = -2776.4 \text{ kJ/mol} \quad (1)$$

Here and below, the reference data[26−29] were used in the calculation of thermochemical quantities; the superscripts (g) and (s) correspond to the gaseous and solid state of the substance, respectively.

In this paper, we investigate the oxidation features of high-density C_4H_4S/O_2 mixtures diluted with argon and water vapor. Table 1 shows the partial pressure of reagents and diluents fed into the reactor, their amount [$n_0(C_4H_4S)$, $n_0(O_2)$, $n_0(D)$, and $n_0(CaCO_3)$], the fuel equivalence ratio φ, and the dilution level x_D of the mixture. As can be seen, tests were carried out with rich, stoichiometric, and lean C_4H_4S/O_2 mixtures (φ = 0.80−1.33) at their dilution level x_D ranging from 35 to 64% mol.

2.1. Oxidation of Thiophene in the Argon Medium in the Presence of a Small Amount of Water Vapor. The oxidation of thiophene in the argon/water vapor medium was studied in C_4H_4S/O_2 stoichiometric mixtures at their dilution levels x_D = 64 and 57% mol (tests 1 and 2, respectively). Figures 1a and 2a show the change in the temperature difference $\Delta T = T_{in} - T_{out}$ as a function of time t and temperature T_{out} during thiophene oxidation in tests 1 and 2, respectively. Here and below, T_{out} corresponds to a given increase in the reactor wall temperature at a rate of 1 K/min, and T_{in} is the temperature of the reaction mixture measured by an internal thermocouple. Note that the initial and final sections of the curves $\Delta T(t, T_{out})$ lie in the negative region of ΔT due to the lag in the temperature of the reaction mixture from the reactor wall temperature during heating.

Table 2 shows the following parameters of the curves $\Delta T(t, T_{out})$ and the reaction mixture: T^*_{out} and T^*_{in} are the temperatures of the reactor wall and the reaction mixture, respectively, at which oxidation begins; T^f_{out} and T^f_{in} are the temperatures corresponding to the end of oxidation and

https://doi.org/10.1021/acsomega.1c00926
ACS Omega 2021, 6, 13134−13143

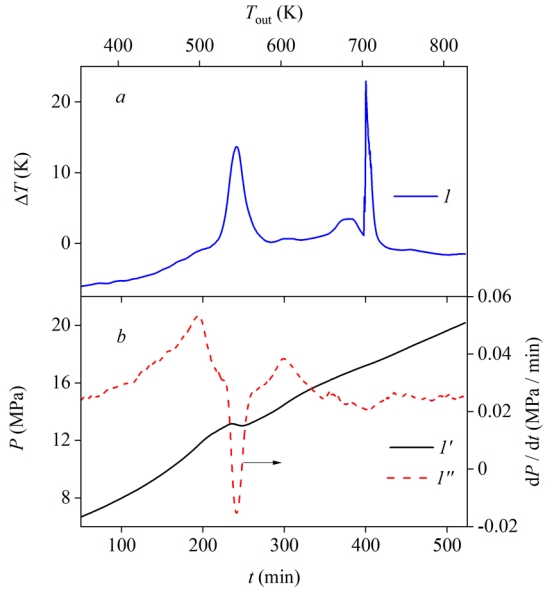

Figure 1. Dependence of the temperature increment ΔT (curve 1) (a), the pressure P (curve 1′) of the reaction mixture, and the rate of pressure change dP/dt (curve 1″) (b) on the time t and the set reactor temperature T_{out} during the oxidation of thiophene in argon with a small amount of water vapor in test 1 (x_D = 64% mol). Time t = 0 corresponds to the start of reactor heating. The numbers of the curves correspond to the numbers of tests in Table 1.

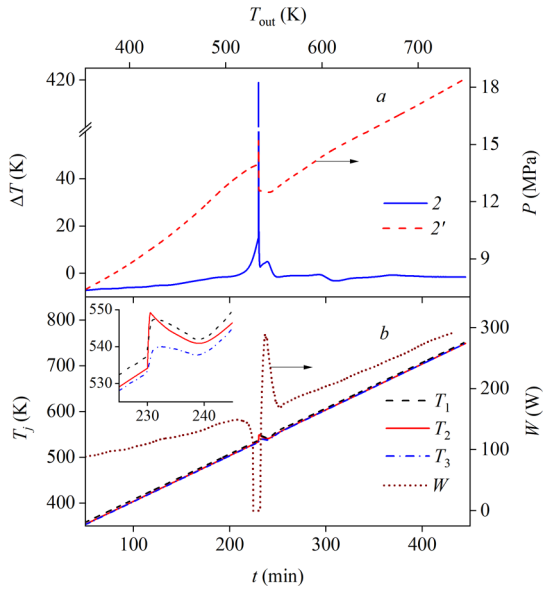

Figure 2. Dependence of the temperature increment ΔT (curve 2) and the pressure P (curve 2′) of the reaction mixture (a); the temperature of the thermocouples T_1−T_3 and the power of the resistive heater W (b) on the time t and set reactor temperature T_{out} during the oxidation of thiophene in argon with a small amount of water vapor in test 2 (x_D = 57% mol). The insert shows a scaled-up area of sharp changes in temperature measured by T_1−T_3 thermocouples. Time t = 0 corresponds to the start of reactor heating. The numbers of the curves correspond to the numbers of tests in Table 1.

reaching the curve of the baseline; t_{ox} is the duration of oxidation; T_{out}^{max} and T_{in}^{max} are the temperatures corresponding to the maximum on the curve $\Delta T(t, T_{out})$; ΔT^{max} is the maximum increase in the temperature of the reaction mixture; ΣC_v is the heat capacity of the reaction mixture at a temperature of 700 K, calculated using the reference data;[26,27,30] ΔT_{ad} is calculated temperature increment of the reaction mixture due to heat release during reaction 1 under adiabatic conditions. The calculation method of the above values is described in detail in some works.[13,14]

It is obvious that in the context of the present work, the temperature T_{in}, recorded by the internal thermocouple, will be determined by the endothermic evaporation processes of thiophene and water (the enthalpy of their evaporation at 400 K is ΔH_{ev} = 29.0 and 39.3 kJ/mol, respectively),[27,30] endothermic decomposition reactions of thiophene and intermediates, and exothermic oxidation reactions in the gas phase and on the surface of the Pt−Rh/Pt thermocouple. The exothermic reactions on the reactor wall almost do not affect the indications of the thermocouple T_{in} due to the high heat capacity C = 548 J/kg·K and the thermal conductivity λ = 21 W/m·K of stainless steel,[31] as well as the stabilizing effect of the thermoprogrammer, which regulates the reactor heating by reducing the heater power. Note that under adiabatic conditions, heat release at complete thiophene oxidation ($n_0(C_4H_4S)$ = 7.6 and 10.1 mmol, Q = 21.1 and 28.0 kJ) in reaction 1 could have led to an increase in the reactor temperature, whose mass was m_r = 3.6 kg, by ≈ 10.7 and 14.2 K, or the temperature of the gas contained in the reactor at homogeneous combustion—by several thousand degrees (Table 2).

The thiophene oxidation onset temperature in tests 1 and 2 is T_{in}^{*} = 419 K and does not depend on the dilution level x_D (Table 2). However, with a further increase in temperature, the thiophene oxidation dynamics in tests 1 and 2 differ. As can be seen in Figure 1a, the dependence $\Delta T(t, T_{out})$ obtained in test 1 has two maxima at T_{out}^{max} = 546 and 705 K (ΔT^{max} = 14 and 23 K, respectively). The first maximum on the curve $\Delta T(t, T_{out})$ corresponds to the minimum of the pressure change rate $dP/dt(t, T_{out})$, while the second more intense maximum is not reflected in the pressure change (Figure 1b). The pressure drop of the reaction mixture against the background of an increase in temperature at T_{out} = 540−552 K is apparently caused by a decrease in the number of reacting species due to condensation reactions, which is consistent with the data.[16] The formation of condensation reaction products was indicated, in particular, by the fact that the surface of the thermocouple (Figure 3a) and the inner surface of the reactor were covered with a uniform layer of soot. According to Zhao *et al.*,[32] the formation and growth of soot particles are promoted by sulfates formed during the combustion of fuel. It is obvious that the second maximum on the curve $\Delta T(t, T_{out})$ is due to the oxidation of thiophene and/or the products resulting from condensation reactions directly on the surface of the Pt−Rh/Pt thermocouple, which does not cause an additional increase in the temperature and pressure of the reaction mixture. Note that the thermal consumption for heating the open section of the thermocouple (the junction diameter was 1.0 mm, the diameter and length of the conductors were 0.35 and 12 mm, respectively) per 100 K were 0.8 J, and corresponded to the heat released during oxidation of ≈0.4 μmol of thiophene in reaction 1. The heat capacity and density of platinum were assumed to be equal to C_{Pt} = 132 J/kg·K and ρ_{Pt} = 21.45 g/cm^3.

Obviously, the oxidation of thiophene directly on the surface of the Pt−Rh/Pt thermocouple results from dissociative adsorption of thiophene and oxygen on the platinum surface.

https://doi.org/10.1021/acsomega.1c00926
ACS Omega 2021, 6, 13134−13143

Table 2. Characteristic Points of Curves in Figures 1, 2, 5, and 7 and Thermodynamic Parameters of the Reaction Mixtures

test (φ; x_D)	T^*_{out} (K)	T^*_{in} (K)	T^f_{out} (K)	T^f_{in} (K)	t_{ox} (min)	T^{max}_{out} (K)	T^{max}_{in} (K)	ΔT^{max} (K)	ΣC_v (J/K)	ΔT_{ad} (K)
Argon + Water Vapor										
1 (1.01; 64)	424	419	799	797	375	705	727	23	3.47	6073
2 (1.01; 57)	424	419	607	604	182	534	953	419	4.21	6675
Water Vapor										
4 (1.33; 46)	427	421	568	565	142	548	548	0	4.11	5133
5 (1.01; 40)	425	419	614	612	189	532	533	1	4.51	6226
6 (0.80; 35)	424	419	738	736	313	648	844	196	4.92	7137
7 (0.80; 35)			715	713		629	753	124	4.92	7137
8 (0.81; 52)	423	417	717	715	294	632	854	222	6.71	5238

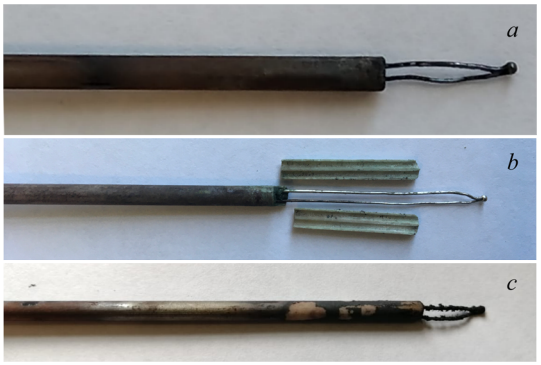

Figure 3. Photos of the Pt−Rh/Pt thermocouple after tests 1 (a), 2 (b), and 5 (c). Photos were taken by one of the authors.

Stöhr *et al.*,[33] when studying the transformation of thiophene on the Pt(111) surface, revealed that the cleavage of the C−S bond and the formation of a metallocycle intermediate occur during chemisorption, in which the S atom is replaced by a Pt surface atom. Using NEXAFS spectroscopy, it was found[34] that the cleavage of the C−S bond begins at 290 K and ends at 470 K; the Pt−S bond remains stable up to 1000 K. Bonzen and Ku,[35] when studying the kinetics of O_2 adsorption on the pure surface of Pt(111) within the temperature range of 486−673 K, revealed that the initial sticking coefficient decreases exponentially with increasing coverage. According to Zyubin *et al.*,[36] upon adsorption onto the platinum surface, the O_2 molecule forms peroxide, where each oxygen atom is bound to a platinum atom. When heated, the O−O bond is broken, and the bound oxygen is stored on the platinum surface.[36] Since the dissociation energy of the O_2 molecule[29] is 498 kJ/mol and the dissociation energy of the Pt−O bond decreases from 405 to 270 kJ/mol with an increase in the coverage of platinum with oxygen,[36] the oxidation of thiophene on the platinum surface occurs at lower activation barrier than in the gas phase.

An increase in the amount of thiophene and oxygen (a decrease in the dilution level x_D) in test 2 (Table 1) led to more intense oxidation compared to test 1. As can be seen in Figure 2a, the oxidation of thiophene in test 2 was accompanied by an explosion. It is obvious that the process was initiated on the surface of the Pt−Rh/Pt thermocouple and then propagated into the gas phase. This contributed not only to an increase in the temperature increment to ΔT^{max} = 419 K (T^{max}_{in} = 953 K) but also to an increase in the reactor wall temperature above the set value. Figure 2b shows the dependence of the temperature of thermocouples T_1−T_3 and the change in the power of the resistive heater W on time t and set temperature T_{out} in test 2. It is seen that at the moment of maximum heat release at T^{max}_{out} = 534 K, the temperature of thermocouples T_1, T_2, and T_3 increased by 8, 15, and 5 K, respectively, relative to the set value. The difference in the temperature increment of thermocouples T_1−T_3 results from the different heat removal and a specific quantity of metal of the reactor parts. When the temperature of thermocouple T_2 increased above the set value, the resistive heater was turned off (W = 0 W), which, due to the lag effect, has led the reactor temperature to decrease below the set value of T_{out} (see the insert in Figure 2b). The subsequent sharp increase in the heater power ensured that the reactor reached the set temperature mode. Based on the fact that the explosion was short-lived and ended with almost complete burning-out of

Table 3. Composition and Amounts of the Products of Thiophene Oxidation in Argon and Water Vapor (mmol)[a]

	argon + water vapor		water vapor				
products	1	2	4	5	6	7	8
Ar	100.6	100.4					
O_2	0.45	0.40	0.40	0.39	7.57	9.76	3.39
CO	0.30	0.40	0.36	0.27	0.32	0.63	0.23
CO_2	26.61	37.46	32.91	36.00	39.17	39.12	37.53
CH_3−CH=CH_2	0.16	0.21	0	0.01	0.01	0	0.01
CH_3−CH_2−CHO	0	0.03	0.02	0.02	0.02	0.02	0.03
CH_2=CH−COOH	0	0	0.01	0.01	0.02	0	0.01
C_4H_4S	0.27	0.06	0.06	0.24	0.14	0.05	0.40
X_C (mol %)	87.5	92.7	81.5	89.1	97.0		92.9
$(CO)_R$	0.18	0.06	0.12	0.32		0.59	0.13
$(CO_2)_R$	0.72	0.81	6.56	1.91		5.25	0.52
Y_C (mol %)	96.6	98.2	99.7	98.0	99.5	113.5	99.4

[a]Subscript R refers to substances produced *via* annealing the reactor at 873 K for 90 min.

https://doi.org/10.1021/acsomega.1c00926
ACS Omega 2021, 6, 13134−13143

thiophene [reducing ΔT to the base level (Figure 2a)], we assumed that in test 2, there was a detonation of the reaction mixture, which was initiated by the occurrence of a shock wave in the near-surface region of the Pt−Rh/Pt thermocouple. The detonation led to the destruction of the ceramic shell of the thermocouple (Figure 3b) and damage to the strain gage transducers, which was manifested in a sharp decrease in its readings after the passage of the shock wave (Figure 2a).

The results of the mass spectrometric analysis of thiophene oxidation products, as well as the values of the degree of carbon burnout X_C and the carbon balance Y_C, calculated from these data, are given in Table 3. Carbon oxides, propene, propanal, and a residual amount of thiophene were found in the composition of the products. Obviously, the presence of C_3H_6 in the products resulted from the decomposition of thiophene on the platinum surface[33] and the presence of C_2H_5CHO as a result of partial oxidation of propene. The presence of a small amount of O_2 and thiophene in the products is due to their residue in capillary connecting the reactor to the adjusting valve. A smaller amount of unreacted thiophene and a larger X_C value was obtained in test 2, where the largest temperature increment ΔT^{max} was detected (Table 2). The maximum loss of carbon (X_C = 96.6% mol) was detected in test 1, which is explained by the significantly larger amount of soot on the thermocouple surface (Figure 3a) and the fact that its annealing was carried out without analysis of gas products (see Section 4).

2.2. Oxidation of Thiophene in the Water Vapor. The transformation of thiophene in water vapor was studied in the absence of O_2, in rich, stoichiometric, and lean C_4H_4S/O_2 mixtures at a dilution level x_D ranging from 35 to 52 mol % (Table 1). Figure 4 shows the temperature dependences of the saturated vapor pressure of water and thiophene, as well as the pressure of water vapor after its complete evaporation in the isochoric process. Based on the values of $n_0(C_4H_4S)$ and $n_0(H_2O)$ (Table 1), the reactor volume occupied by gas, and the reference $P-\rho-T$ data,[27,37] it is easy to estimate that thiophene will completely transfer into the gas phase at T_{ev} = 424 K, while water—at T_{ev} = 502 (tests 3−7) and 542 K (test 8). As can be seen in Figure 4, at T < 444 K, the partial pressure and hence the density of saturated thiophene vapor is greater than that of water vapor. From these data, it also follows that part of the heat released during the oxidation of thiophene will be spent on its evaporation and evaporation of water up to T_{ev}.

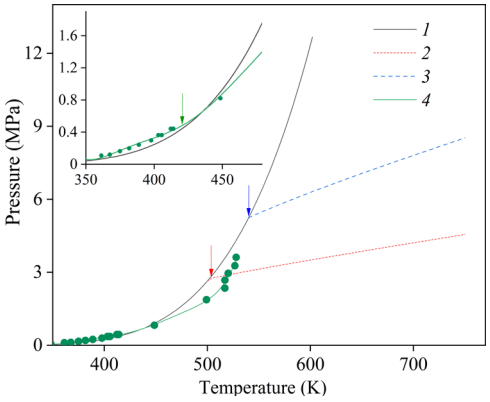

Figure 4. Temperature dependences of the saturated vapor pressure of water (1) and thiophene (4), the water vapor pressure corresponding to the density $\rho(H_2O)$ = 0.761 (2) and 1.481 mol/dm^3 (3), plotted based on the reference $P-\rho-T$ data.[27,37] The insert shows a scaled-up temperature range of 350−475 K. The arrows indicate the conditions corresponding to the complete evaporation of water and thiophene.

Dependences of the increments of temperature, the pressure of the reaction mixture, and the rate of pressure change on time and set reactor temperature in tests 3−5 are shown in Figure 5. Here also shown are the dependencies 3° that characterize the behavior of the reaction system in the absence of thiophene and oxygen (in test 3°, the reactor was filled with water and nitrogen; see Section 4). From a comparison of the dependencies $\Delta T(t, T_{out})$, it can be seen (Figure 5a) that curve 3 is located above curve 3° up to 770 K. Obviously, this is due to the greater thermal conductivity of the $C_4H_4S/H_2O/N_2$ mixture than the H_2O/N_2 mixture. The dip in curve 3, as well as in curves 4 and 5, within the temperature range of 380−420 K can be associated with the evaporation of thiophene. The smaller dip in curves 4 and 5 than in curve 3 is the result of the superposition of endothermic evaporation and exothermic oxidation. The type of dependencies $P(t, T_{out})$ and $dP/dt(t, T_{out})$, obtained in test 3 corresponds to a larger number of species in the gas phase and a higher rate of pressure increase due to thiophene evaporation at T < 424 K than in test 3° (Figures 5b,c). The maximum of the dP/dt derivative (curves 3 and 3°) corresponds to the complete evaporation of water.

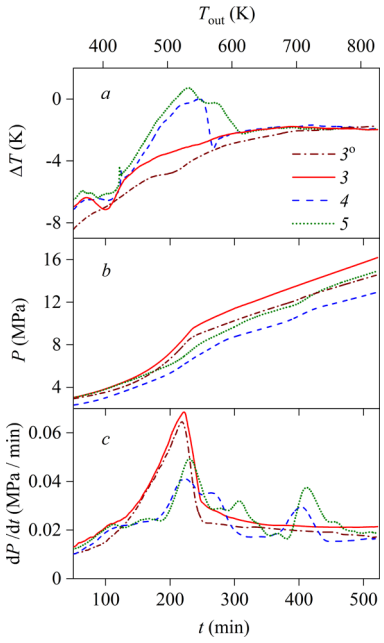

Figure 5. Dependence of the temperature increment ΔT (a), the pressure P of the reaction mixture (b), and the rate of pressure change dP/dt (c) at time t and the set reactor temperature T_{out} during gasification (test 3) and oxidation of thiophene in water vapor in tests 4 and 5 (φ = 1.33 and 1.01, respectively). Curves 3° characterize the system's behavior in the absence of thiophene. Time t = 0 corresponds to the start of reactor heating. The numbers of the curves correspond to the numbers of tests in Table 1.

The gas products formed in test 3 include the following components (mmol): H_2—0.02, CH_4—0.01, CO—0.03, and CO_2—0.12. The absence of H_2S in the composition of volatile products may be due to both its solubility in water (0.378 wt % at 298 K)[38] and sulfidation of the reactor wall.[39] The degree of

https://doi.org/10.1021/acsomega.1c00926
ACS Omega 2021, 6, 13134−13143

thiophene conversion (≈0.4% mol), calculated based on the amount of CO_2, CO, and CH_4, turned out to be an order of magnitude less than in the works.[18,19] One of the reasons for this could be the polymerization of thiophene on the surface of the reactor wall at the initial stage of its heating. As established by Cheng *et al.*,[40] upon adsorption on the iron surface, thiophene loses both H atoms at position 2 relative to the sulfur atom, which leads to its polymerization and desorption of H_2. Harraz *et al.*[41] observed the formation of a polythiophene layer on the surface of α-Fe_2O_3 nanoparticles. Our assumption is also based on the fact that after opening the reactor, a dark bloom was detected on its wall (not observed in other tests), which could be removed only after repeated annealing and mechanical cleaning.

At oxidation of thiophene in water vapor (tests 4 and 5), the temperature increment ΔT^{max} was significantly less than that at oxidation in argon with a small amount of water vapor (test 2). At the same time, the temperature of the thiophene oxidation onset in tests 5 and 2 coincided (T^*_{in} = 419 K), while in test 4, it was slightly higher (T^*_{in} = 421 K) due to the lower amount of $n_0(O_2)$ (Tables 1 and 2). An increase in the amount of $n_0(O_2)$ in test 5 increased the contribution of homogeneous reactions, as indicated by an increase in the oxidation time t_{ox} and the area under the curve $\Delta T(t, T_{out})$ (Figure 5a). As in tests 3 and 3°, the presence of the first maxima on the $dP/dt(t, T_{out})$ curves (Figure 5c), obtained in tests 4 and 5, is associated with complete evaporation of water. The second maxima on curves 4 and 5 at T_{out} = 703−723 K, respectively, characterize the oxidation of the products of condensation reactions. The composition of the oxidation products obtained in tests 4 and 5 was almost the same, except for a larger amount of unburned thiophene in test 4 [see X_C and $(CO_2)_R$ values in Table 3]. In contrast to the results of Khalil *et al.*,[22] maleic acid and SO_2 were not detected in the products obtained in tests 4 and 5, which is explained by their further oxidation by a water−oxygen mixture to acrylic acid (eventually to CO_2) and H_2SO_4, respectively. As can be seen in Figure 3, the soot particle size in test 5 was larger than in tests 1 and 2, apparently due to the larger amount of sulfates formed.[32]

Comparison of the thiophene oxidation in tests 2 and 5, corresponding to the same amount of $n_0(C_4H_4S)$ and $n_0(O_2)$ (Table 1), indicates that the contribution of homogeneous oxidation reactions in water vapor is significantly less than in argon (Figures 2a and 5a). This can be assumed to be caused not only by the higher heat capacity of water vapor,[27] which prevents the development of intense combustion, but also by the involvement of H_2O molecules in the heterogeneous oxidation of thiophene on the surface of the reactor wall (the surface of iron oxides). As noted by Khalil *et al.*,[22] upon the oxidation of thiophene by lattice oxygen from hematite, the latter is transformed into magnetite; however, due to interaction with water, magnetite again is transformed into hematite. A similar conclusion was made by Hosseinpour *et al.*[42] based on the research results of the SCW conversion of heavy oil in the presence of iron oxide nanoparticles. Even though in the present work, the inner surface of the reactor was annealed in an atmosphere of O_2 (see Section 4) to obtain the oxide layer before each test, the formation of Fe_xO_y could also be caused by the oxidation of iron with water[43] or a water−oxygen mixture. Besides, in this work, the $Fe_3O_4 \rightarrow Fe_2O_3$ transition could have also occurred in the reaction of magnetite with molecular or atomic oxygen. Note that both magnetite and hematite were detected in corrosion products isolated from the reactor after the end of the tests (see below). This means that in the present study, heterogeneous catalytic oxidation of thiophene occurred on the surface of both the Pt−Rh/Pt thermocouple and the reactor wall (iron oxides) in a Fenton-like process.[44] We also do not exclude the effect of other metals (*e.g.*, chromium) contained in stainless steel on the oxidation reactions. However, based on the results of a study of SCW oxidation of aromatic compounds in the presence of a Cr_2O_3/Al_2O_3 catalyst[45] and data on the stability of Cr_2O_3 in this process,[46] it follows that the contribution of chromium oxides to the oxidation of thiophene is secondary.

The dependences of the temperature increment, the pressure of reaction mixture, and the rate of pressure change on the time and set reactor temperature in tests 6−8 conducted with the lean C_4H_4S/O_2 mixtures are shown in Figure 6. Test 7 differs from test 6 by the presence of $CaCO_3$

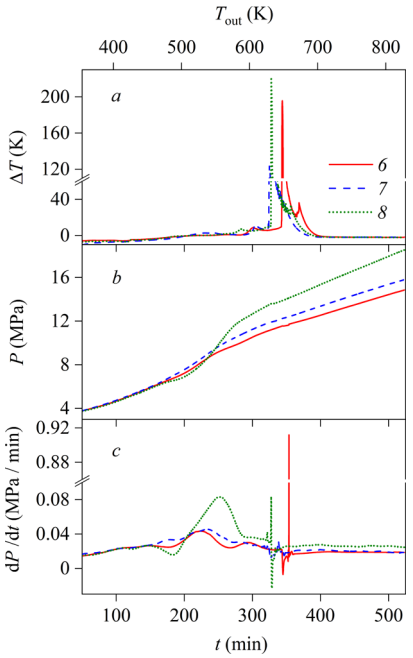

Figure 6. Dependence of the temperature increment ΔT (a), the pressure P of the reaction mixture (b), and the rate of pressure change dP/dt (c) on time t and the set reactor temperature T_{out} during the oxidation of thiophene in water vapor in tests 6, 7, and 8 (x_D = 35, 35, and 52% mol, respectively). Time t = 0 corresponds to the start of reactor heating. The numbers of the curves correspond to the numbers of tests in Table 1.

in the reaction system, while test 8 differs from test 6 by a twofold increase in the amount of water. As it follows from the data shown in Figures 5 and 6, the thiophene oxidation dynamics in tests 6−8 differs from that in tests 4 and 5, primarily by a longer duration of oxidation t_{ox} and a larger temperature increment ΔT^{max} (Table 2). It is obvious that the latter proceeds from an increase in the O_2 content in the reaction mixture and, as a consequence, an increase in the degree of platinum coverage with oxygen, resulting, according to O'Brein *et al.*,[47] to increase the oxidation rate. As a result, the maximum temperature increment in tests 6, 7, and 8 was ΔT^{max} = 196, 124, and 222 K, respectively. Moreover, in tests 6 and 8, this increment in temperature was reflected in the time dependences of pressure (Figures 6b,c). At the same time,

https://doi.org/10.1021/acsomega.1c00926
ACS Omega 2021, 6, 13134−13143

unlike test 2 (Figure 2b), the reactor wall temperature did not exceed the set value of T_{out}.

The lower value of ΔT^{max} in test 7, than in tests 6 and 8, is explained by the greater contribution of heterogeneous oxidation of thiophene on the surface of the cell with $CaCO_3$. We were not able to reliably determine the oxidation onset temperature T_{in}^{*} and, accordingly, the duration of oxidation t_{ox} in test 7 due to the high heat consumption for heating the cell and the predominance of heterogeneous oxidation, which was not recorded by the T_{in} thermocouple. Despite the larger amount of water filled into the reactor, the maximum temperature increment ΔT^{max} in test 8 was greater, and the flash occurred at a lower temperature, T_{out}^{max}, than in test 6 (Tables 1 and 2). This may be because an increase in the density of water vapor suppresses heterogeneous reactions on the reactor wall (the metal oxide's surface) due to the adsorption of water molecules.[48] In general, a comparison of the $\Delta T(t, T_{out})$ curves obtained during the oxidation of thiophene in water vapor allows concluding that with oxygen deficiency and a stoichiometric amount of O_2, reactions on the surface of the reactor wall predominate, while with an excess of O_2, reactions on the surface of the Pt−Rh/Pt thermocouple become dominant.

The results of the mass spectrometric analysis of gas products (Table 3) show that an increase in the O_2 content in the reaction mixture from test 4 to test 6 (φ = 1.33−0.80) leads to an increase in the degree of carbon burnup from 81.5 to 97% mol. However, an increase in the water density in test 8 contributes to a decrease in the X_C value to 92.9%. The largest amount of unreacted O_2 and substances formed during annealing of the reactor was obtained in test 7, which is due to the presence of a cell with $CaCO_3$ in the reactor. It is obvious that the excess of the Y_C over 100% in test 7 was caused by the release of CO_2 resulting from the neutralization of sulfuric acid with calcium carbonate. Based on the values of Y_C and $n_0(C_4H_4S)$, it is easy to calculate that only 54% of the amount of sulfuric acid formed by reaction 1 has transformed into $CaSO_4$ (Figure 7). However, the corrosion of stainless steel has noticeably decreased.

Figure 8 shows the phase composition of corrosion products formed during the oxidation of thiophene in water vapor and subsequent annealing of the reactor in tests 4 and 7. In addition to chromium ferrite, magnetite, hematite, nickel sulfate, iron sulfate, and hydroxy sulfate, shown in the form of bar charts in Figure 8b−g, the following products were detected: chromite, Cr_2FeO_4 (PDF card 00-024-0512); chromium oxide, Cr_2O_3 (PDF Card 00-059-0308); and chromium sulfate, $CrSO_4$ (PDF card 00-021-0244). A comparison of the XRD patterns obtained in tests 4 and 7 shows that in the latter case, the relative intensity of the bands corresponding to nickel and iron sulfates is significantly less. The presence of iron, nickel, and chromium sulfates in corrosion products can be a consequence of the interaction of sulfuric acid with both the oxide layer on the surface of the reactor wall and directly with stainless steel. Studies of corrosion of the nickel alloy in an aqueous solution of sulfuric acid ($T \leq 773$ K, $P \leq 38$ MPa) have shown[49] that the most intense corrosion occurred in liquid water at 423−503 K due to the dissolution of the oxide layer; at $T > 503$ K, the alloy surface was passivated, and the corrosion rate significantly decreased. As applied to the results of the present work, this means that the bulk of iron, nickel, and chromium sulfates was formed after the end of the test during the cooling of the reactor. Therefore, the discharge of the hot reaction mixture from the reactor and/or the addition of neutralizing agents (hydroxides and carbonates of alkaline or alkaline earth metals) into the reactor will reduce the corrosion of structural materials.

It should be noted that some features of the thiophene oxidation in water vapor, detected in this work, were observed by us during the oxidation of dibenzothiophene under similar conditions.[15] However, due to the greater resistance of dibenzothiophene to oxidation and the low pressure of its saturated vapor, these features were manifested poorly, which required further research on the oxidation of thiophene as the simplest aromatic S-containing compound. This resulted in obtaining reliable data that broaden the understanding of the oxidation mechanisms of thiophene derivatives in dense water vapor.

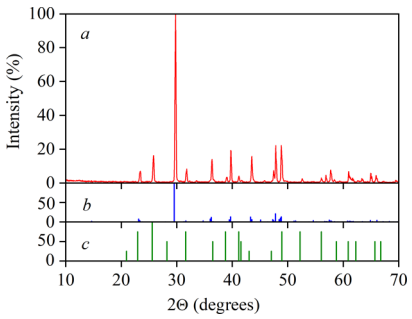

Figure 7. X-ray diffraction (XRD) pattern of the sample taken from the cell after oxidation of thiophene in water vapor and subsequent annealing of the reactor in test 7 (a). Bar charts show the reference data[51] for (b) calcium carbonate, $CaCO_3$ (monoclinic, PDF card 04-012-8783); (c) anhydrite, $CaSO_4$ (orthorhombic, PDF card 00-003-0377).

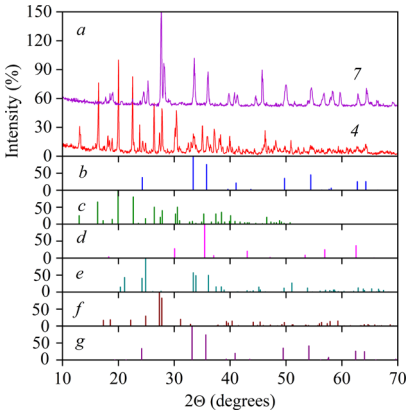

Figure 8. XRD patterns of corrosion products resulted during the oxidation of thiophene in water vapor and subsequent annealing of the reactor after tests 4 and 7 (a). Bar charts show the reference data[51] for (b) chromium ferrite, $CrFeO_3$ (rhombohedral, PDF card 04-006-8200); (c) nickel sulfate hydrate, $NiSO_4{\cdot}4H_2O$ (monoclinic, PDF vard 00-019-0843); (d) magnetite, $Fe_{2.964}O_4$ (cubic, PDF card 04-009-2283); (e) iron sulfate, $FeSO_4$ (orthorhombic, PDF card 04-005-6737); (f) iron hydroxy sulfate, $Fe(SO_4)(OH)$ (orthorhombic, PDF card 04-012-6256); (g) hematite, Fe_2O_3 (rhombohedral, PDF card 04-006-6579).

https://doi.org/10.1021/acsomega.1c00926
ACS Omega 2021, 6, 13134−13143

3. CONCLUSIONS

In this research, the oxidation of thiophene in argon and water vapor at high reagent density is studied for the first time. The experimental method is based on measuring the time dependences of the reaction mixture temperature using a Pt−Rh/Pt thermocouple inserted into the center of the reaction volume at uniform slow heating of the reactor. It is established that the oxidation of thiophene in the argon and water vapor media proceeds according to homogeneous (in the volume of the reaction mixture) and heterogeneous (on the surface of the reactor wall and Pt−Rh/Pt thermocouple) reactions. In the water vapor medium, under oxygen deficiency and at a stoichiometric amount of O_2, heterogeneous oxidation of thiophene on the surface of the reactor wall (primarily iron oxides) prevails. The increase in water vapor density suppresses heterogeneous reactions on the reactor wall, apparently, due to the adsorption of water molecules. With an excess of O_2 in the water vapor medium and a stoichiometric amount of O_2 in the argon medium, thiophene oxidation dominates on the surface of the Pt−Rh/Pt thermocouple. In the case of the high density of the reagents, the latter can lead to detonation combustion regimes. It is shown that sulfuric acid formed during the oxidation of thiophene in water vapor causes corrosion of stainless steel that can be reduced by adding $CaCO_3$. The results obtained show the need to take into account heterogeneous processes occurring on the reactor wall when developing technologies for processing heavy oil raw materials in SCW or dense water vapor, especially in the case of using concentrated solutions and/or reactors with a large ratio of the reactor wall surface to its volume.

4. MATERIALS AND METHODS

The experiments were carried out using the test facility described in detail in works.[13,14] A schematic sketch of the reactor is shown in Figure 9. The reactor (with an internal diameter of 30 mm, a length of 90 mm, and wall thickness of 15 mm) and structural elements were made of stainless steel (analogue to AISI 321H). The reactor was located in a cylindrical furnace heated by a resistive heater. The heating rate was controlled by a thermoprogrammer equipped with a PID controller and a chromel−alumel thermocouple T_2 mounted on the outer wall of the reactor. Additionally, the reactor temperature was measured by two chromel−alumel thermocouples T_1 and T_3 located at its butt ends. The temperature of the reaction mixture T_{in} was measured by a Pt−Rh/Pt thermocouple (type S) inserted into the center of the reaction volume through the butt end of the reactor. The choice of Pt−Rh/Pt thermocouple to measure temperature was due to its corrosion resistance in an oxidizing S-containing atmosphere. The Pt−Rh/Pt thermocouple was placed in a corundum two-channel tube 2 (with an outer diameter of 3 mm). The open end of the thermocouple protruded from the corundum tube by 13 mm and was located in the center of the reaction volume. The pressure of the reagents was measured by a strain gauge transducer 9 (with a measurement limit of 100 MPa). The temperature and pressure measurement errors were ±0.5 K and ±0.03 MPa, respectively. Time dependences of temperature and pressure were recorded in the digital form with a frequency of 10 Hz. Reagents were fed into the reactor through a capillary 5 welded into the central part of the reactor sidewall through an adjusting valve 6. The reactor volume inside the furnace (reaction volume) was 65.7 cm^3, while the reactor volume outside the furnace (the channel for entering the thermocouple into the reactor and the capillaries connecting the reactor to the adjusting and shut-off valves) was 1.4 cm^3. Before feeding with reagents, the reactor was evacuated using a prevacuum pump.

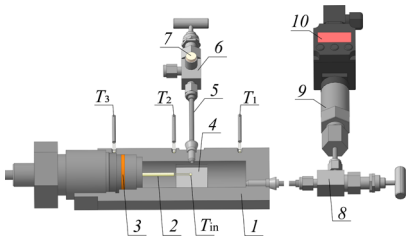

Figure 9. Schematic sketch of the test facility: reactor (1); two-channel corundum tube (2); thermocouple inserted into the reactor (T_{in}); measuring thermocouples (T_1, T_3); controlling thermocouple (T_2); sealing copper gasket (3); a cell with $CaCO_3$ (4); capillary for the input of reagent (5); adjusting valve (6); rubber membrane for the input of liquid reagent (7); shut-off valve (8); strain gauge transducer (9); indicator communicator to pressure sensor (10).

The following reagents were used in tests: thiophene (99%, Alfa Aesar), oxygen (99.95% vol), argon (99.99% vol), nitrogen (99.95% vol), calcium carbonate (>99.9%), and distilled water. In tests 1 and 2, where argon was used as a diluent of the C_4H_4S/O_2 mixture, the nonheated reactor volumes were filled with water to prevent condensation of thiophene (the boiling point T_b = 357.3 K).[30] To do this, water (3.0 cm^3) was filled into the reactor using a syringe through a rubber membrane 7 installed on the nipple of the reagent supply valve 6 (Figure 9). The reactor was then heated to a temperature T_2 = 403 K and thermostated for 45 min. During this time, a certain portion of the water (≈1.4 cm^3) was recondensed into nonheated volumes of the reactor. Then, at T_{in} = 403 K, the excess water was discharged from the reactor to a pressure of 0.1 MPa (saturated water vapor pressure at 298 K), which allowed the water to be kept in nonheated volumes. After cooling the reactor to T_{in} = 303 K, it was filled with 0.6 or 0.8 cm^3 of thiophene (with a density of 1.059 g/cm^3 at 298 K)[26] and then, argon and oxygen to a given pressure.

Tests 3° and 3 were calibration tests performed without adding O_2 to the reaction system. In these tests, N_2 was used as a buffer gas since its thermophysical properties[27] are close to those of O_2. The amount of N_2 (≈66 mmol) charged into the reactor corresponded to the amount of O_2 required for complete oxidation of thiophene. In tests 3° and 3, after filling the reactor with water (1.8 cm^3), it was heated to T_2 = 403 K and kept at this temperature for 45 min (at that, a certain portion of the water (≈1.4 cm^3) was recondensed into nonheated volumes). In test 3°, after cooling the reactor to T_{in} = 302 K, it was filled with 0.5 cm^3 of water and nitrogen to a pressure of 2.52 MPa. In test 3, after cooling the reactor to T_{in} = 303 K, 0.8 cm^3 of thiophene, 0.5 cm^3 of water, and nitrogen were successively filled to a pressure of 2.58 MPa. In tests 4−8, the reactor filling procedure was similar to that in test 3. To fill nonheated volumes, 1.8 cm^3 (tests 4−7) and 2.7 cm^3 (test 8) of water were filled into the reactor. After heating the reactor to T_2 = 403 K, holding at this temperature for 45 min, and cooling down to T_{in} = 303 K, 0.8 cm^3 of thiophene, 0.5 cm^3 of water, and oxygen were successively fed into the reactor to a

https://doi.org/10.1021/acsomega.1c00926
ACS Omega 2021, 6, 13134−13143

given pressure, that is, in tests 4−7 and 8, the heated part of the reactor contained ≈50 and 100 mmol of water, respectively. In test 7, thiophene oxidation was conducted in the presence of $CaCO_3$. Calcium carbonate was fed into the reactor in a square cell 4 (with a length of 25 mm, and wall height of 5 mm) made of 0.2 mm thick stainless-steel sheet. After filling with reagents, the reactor was heated to 823 K at a rate of 1 K/min.

The amounts of reagents and diluent were determined based on their temperature and partial pressure, as well as the reactor volume using the reference $P-\rho-T$ data.[27] The value of $n_0(CaCO_3)$ corresponds to two times the amount of $CaCO_3$ required to neutralize sulfuric acid resulting from thiophene oxidation during the reaction

$$CaCO_3^{(s)} + H_2SO_4^{(g)} \rightarrow CaSO_4^{(s)} + H_2O^{(g)} + CO_2^{(g)},$$
$$\Delta_r H^\circ_{298} = -118\ \text{kJ/mol} \quad (2)$$

The choice of $CaCO_3$ as a neutralizing agent is due to its low solubility in water ($1.4\cdot10^{-2}$ g/dm^3 at 298 K).[38]

After turning off the heating, the reactor in the furnace was cooled to room temperature for more than 12 h. Then, the composition and amount of volatile oxidation products were determined using the MS 7303 mass spectrometer according to the method.[50] The amount of carbon in the composition of nonreacted substances was determined as follows. The reactor was charged with oxygen (≈50 mmol), heated to 873 K, and kept at this temperature for 90 min. After cooling the reactor to room temperature, a mass-spectrometric analysis of volatile products was carried out. The carbon burnup degree X_C and carbon balance Y_C were calculated according to the formulae

$$X_C\ (\%) = 100\cdot n(CO_2)/4n_0(C_4H_4S) \quad (3)$$

$$Y_C\ (\%) = 100\cdot\left[\sum jn(C_j) + n(CO_2)_R + n(CO)_R\right]/4\ n_0(C_4H_4S) \quad (4)$$

where $n(C_j)$ is the number of moles of the carbon-containing substance, detected during the mass spectrometric analysis; j is the stoichiometric coefficient; subscript R corresponds to the products obtained upon annealing of the reactor at 873 K.

Since in the context of this work, corrosion of the reactor wall occurred, before running each test, the inner surface of the reactor and the heated parts of the setup were mechanically cleaned of the corrosion layer. Then, to obtain a dense oxide layer, the inner surface of the reactor was annealed in an O_2 environment (≈0.7 MPa at 298 K) at a temperature of 873 K for 60 min. Due to the interaction with the reaction mixture, a bloom appeared on the Pt−Rh/Pt thermocouple. This bloom was removed by annealing the thermocouple and ceramic shell in a muffle furnace in the air at 1103 K for 100 min. Note that the temperature T_{in} in all the tests was measured using just a single Pt−Rh/Pt thermocouple. The composition of solid products was analyzed using a powder X-ray diffractometer X'TRA Thermo (phase identification was carried out according to the reference data[51]).

AUTHOR INFORMATION

Corresponding Author

Oxana N. Fedyaeva − *Kutateladze Institute of Thermophysics SB RAS, Novosibirsk 630090, Russia;* orcid.org/0000-0003-3088-5404; Email: fedyaeva@itp.nsc.ru

Authors

Andrey V. Shishkin − *Kutateladze Institute of Thermophysics SB RAS, Novosibirsk 630090, Russia*

Anatoly A. Vostrikov − *Kutateladze Institute of Thermophysics SB RAS, Novosibirsk 630090, Russia;* orcid.org/0000-0001-6177-4876

Complete contact information is available at: https://pubs.acs.org/10.1021/acsomega.1c00926

Notes

The authors declare no competing financial interest.

ACKNOWLEDGMENTS

The work was supported by the Russian Foundation for Basic Research (grant number 18-29-06005). The authors thank M. Y. Sokol for mass spectrometric analysis of gas products and D. A. Yatsenko for XRD analysis of samples.

REFERENCES

(1) Javadli, R.; de Klerk, A. Desulfurization of Heavy Oil. *Appl. Petrochem. Res.* **2012**, *1*, 3−19.

(2) Fedyaeva, O. N.; Antipenko, V. R.; Vostrikov, A. A. Conversion of Sulfur-Rich Asphaltite in Supercritical Water and Effect of Metal Additives. *J. Supercrit. Fluids* **2014**, *88*, 105−116.

(3) Fedyaeva, O. N.; Antipenko, V. R.; Dubov, D. Y.; Kruglyakova, T. V.; Vostrikov, A. A. Non-isothermal Conversion of the Kashpir Sulfur-Rich Oil Shale in a Supercritical Water Flow. *J. Supercrit. Fluids* **2016**, *109*, 157−165.

(4) Kovalenko, E. Y.; Gerasimova, N. N.; Sagachenko, T. A.; Min, R. S.; Patrakov, Y. F. Characteristics of Products of Thermal Decomposition of Heavy Oil Asphaltenes under Supercritical Conditions. *Energy Fuels* **2020**, *34*, 9563−9572.

(5) Wake, H. Oil Refineries: a Review of Their Ecological Impacts on the Aquatic Environment. *Estuar. Coast Shelf Sci.* **2005**, *62*, 131−140.

(6) Tang, J.; Wang, M.; Wang, F.; Sun, Q.; Zhou, Q. Eco-toxicity of Petroleum Hydrocarbon Contaminated Soil. *J. Environ. Sci.* **2011**, *23*, 845−851.

(7) Lighty, J. S.; Veranth, J. M.; Sarofim, A. F. Combustion Aerosols: Factors Governing Their Size and Composition and Impactions to Human Health. *J. Air Waste Manag. Assoc.* **2000**, *50*, 1565−1618.

(8) Ferek, R. J.; Hobbs, P. V.; Herring, J. A.; Laursen, K. K.; Weiss, R. E.; Rasmussen, R. A. Chemical Composition of Emissions from the Kuwait Oil Fires. *J. Geophys. Res.* **1991**, *97*, 14483−14489.

(9) Rocha, D. H. D.; Silva, R. J. Exergoenvironmental Analysis of an Ultra-Supercritical Coal-Fired Power Plants. *J. Clean. Prod.* **2019**, *231*, 671−682.

(10) Cui, C.; Li, Y.; Wang, S.; Ren, M.; Yang, C.; Jiang, Z.; Zhang, J. Review on an Advanced Combustion Technology: Supercritical Hydrothermal Combustion. *Appl. Sci.* **2020**, *10*, 1645.

(11) Wang, T.; Xiang, B.; Liu, J.; Shen, Z. Supercritical Water Oxidation of Sulfide. *Environ. Sci. Technol.* **2003**, *37*, 1955−1961.

(12) Ma, H. H.; Wang, S. Z.; Zhou, L. Sulfur transformations during supercritical water oxidation of methanthiol and thiirane. *Adv. Mater. Res.* **2012**, *610−613*, 1377−1380.

(13) Fedyaeva, O. N.; Artamonov, D. O.; Vostrikov, A. A. Effect of H_2O and CO_2 on Propane, Propene, and Isopropanol Oxidation at Elevated Pressure. *Combust. Flame* **2019**, *199*, 230−240.

(14) Fedyaeva, O. N.; Artamonov, D. O.; Vostrikov, A. A. Heterogeneous−Homogeneous Oxidation of Pyrrole in Water Vapor at Elevated Pressure. *Combust. Flame* **2019**, *210*, 183−192.

(15) Fedyaeva, O. N.; Shishkin, A. V.; Vostrikov, A. A. Oxidation of Dibenzothiophene in Water Vapor and Argon at Increased Pressure. *J. Eng. Thermophys.* **2020**, *29*, 549−560.

(16) Winkler, J. K.; Karow, W.; Rademacher, P. Gas-Phase Pyrolysis of Heterocyclic Compounds, Part 1 and 2: Flow Pyrolysis and Annulation Reactions of Some Sulfur Heterocycles: Thiophene,

Benzo[b]thiophene, and Dibenzothiophene. A Product-Oriented Study. *J. Anal. Appl. Pyrolysis* **2002**, *62*, 123−141.
(17) Katritzky, A. R.; Barcock, R. A.; Balasubramanian, M.; Greenhill, J. V.; Siskin, M.; Olmstead, W. N. Aqueous High-Temperature Chemistry of Carbo- and Heterocycles. 21. Reactions of Sulfur-Containing Compounds in Supercritical Water at 460°C. *Energy Fuels* **1994**, *8*, 498−506.
(18) Patwardhan, P. R.; Timko, M. T.; Class, C. A.; Bonomi, R. E.; Kida, Y.; Hernandez, H. H.; Tester, J. W.; Green, W. H. Supercritical Water Desulfurization of Organic Sulfides is Consistent with Free-Radical Kinetics. *Energy Fuels* **2013**, *27*, 6108−6117.
(19) Qi, W.; Li, Y.; Liu, Z.; Li, X.; Jiang, Y.; Sun, H. Decomposition Mechanism of Thiophene Compounds in Heavy Oil under Supercritical Water. *Chem. Eng. Sci.* **2020**, *228*, 115979.
(20) Timko, M. T.; Ghoniem, A. F.; Green, W. H. Upgrading and Desulfurization of Heavy Oils by Supercritical Water. *J. Supercrit. Fluids* **2015**, *96*, 114−123.
(21) Kang, J.; Sim, S.; Jung, H.; Han, B.; Lee, Y.-W. Desulfurization of Hexyl Sulfide and Hexanethiol Using Supercritical Water. *J. Supercrit. Fluids* **2020**, *158*, 104734.
(22) Khalil, M.; Lee, R. L.; Liu, N. Hematite Nanoparticles in Aquathermolysis: a Desulfurization Study of Thiophene. *Fuel* **2015**, *145*, 214−220.
(23) Yoshida, S.; Takewaki, K.; Miwa, K.; Wakai, C.; Nakahara, M. Desulfurization of Thiophene in Alkaline Supercritical Water Studied by ^{1}H and ^{13}C NMR. *Chem. Lett.* **2004**, *33*, 330−331.
(24) Song, X.; Fanelli, M. G.; Cook, J. M.; Bai, F.; Parish, C. A. Mechanisms for the Reaction of Thiophene and Methylthiophene with Singlet and Triplet Molecular Oxygen. *J. Phys. Chem. A* **2012**, *116*, 4934−4946.
(25) Zhang, Y.; Wang, R. Recent Advances on Catalyst and Systems for the Oxidation of Thiophene Derivatives in Fuel Oil with Molecular Oxygen. *Mini-Rev. Org. Chem.* **2018**, *15*, 488−497.
(26) Antón, V.; Artigas, H.; Lomba, L.; Giner, B.; Lafuente, C. Thermophysical Properties of the Thiophene Family. *J. Therm. Anal. Calorim.* **2016**, *125*, 509−518.
(27) *Thermophysical Properties of Fluid Systems. NIST Chemistry WebBook, NIST Standard Reference Database No 69*; Lemmon, E. W., McLinden, M. O., Friend, D. G., Linstrom, P. J., Mallard, W. G., Eds.; National Institute of Standards and Technology: Gaithersburg MD, 20899, 2018; http://webbook.nist.gov/chemistry/fluid/.
(28) Hubbard, W. N.; Scott, D. W.; Frow, F. R.; Waddington, G. Thiophene: Heat of Combustion and Chemical Thermodynamics Properties. *J. Am. Chem. Soc.* **1955**, *77*, 5855−5857.
(29) Lidin, P. A.; Andreeva, L. L.; Molochko, V. A. *The Constants of Inorganic Compounds: Handbook*; Drofa: Moscow, 2006; [In Russian].
(30) *NIST Chemistry WebBook. NIST Standard Reference Database Number 69*; Linstrom, P. J., Mallard, W. G., Eds.; National Institute of Standards and Technology: Gaithersburg MD, 20899, 2018; https://webbook.nist.gov/chemistry/.
(31) Guva, A. Y. *Brief Thermophysical Handbook*; Sibvuzizdat: Novosibirsk, 2002; [In Russian].
(32) Zhao, Y.; Ma, Q.; Liu, Y.; He, H. Influence of Sulfur in Fuel on the Properties of Diffusion Flame Soot. *Atmos. Environ.* **2016**, *142*, 383−392.
(33) Stöhr, J.; Gland, J. L.; Kollin, E. B.; Koestner, R. J.; Johnson, A. L.; Muetterties, E. L.; Sette, F. Desulfurization and Structural Transformation of Thiophene on the Pt(111) Surface. *Phys. Chem. Lett.* **1984**, *53*, 2161−2164.
(34) Khan, N. A.; Hwu, H. H.; Chen, J. G. Low-Temperature Hydrodesulfurization of Thiophene on Ni/Pt(111) Bimetallic Surfaces with Monolayer Ni Coverage. *J. Catal.* **2002**, *205*, 259−265.
(35) Bonzel, H. P.; Ku, R. On the Kinetics of Oxygen Adsorption on a Pt(111) Surface. *Surf. Sci.* **1973**, *40*, 85−101.
(36) Zyubin, A. S.; Zyubina, T. S.; Dobrovol'skii, Y. A.; Volokhov, V. M. Oxygen Behavior on the Platinum Surface: a Quantum-Chemical Modeling. *Russ. J. Inorg. Chem.* **2013**, *58*, 803−807.
(37) Daubert, T. E.; Hutchison, G. *Vapor Pressure of 18 Pure Industrial Chemicals*; AIChE Symposium Series; ACS, 1990; Vol. *86*, pp 93−114.
(38) *Perry's Chemical Engineers' Handbook*, 7th ed.; Perry, R. H., Green, D. W., Maloney, J. O.; McGraw-Hill: New York, 1997.
(39) Fedyaeva, O. N.; Vostrikov, A. A. Disposal of Hazardous Organic Substances in Supercritical Water. *Russ. J. Phys. Chem. B* **2012**, *6*, 844−860.
(40) Cheng, L.; Bocarsly, A. B.; Bernasek, S. L.; Ramanarayanan, T. A. Adsorption and Reaction of Thiophene on the Fe(100) Surface: Selective Dehydrogenation and Polymerization. *Surf. Sci.* **1997**, *374*, 357−372.
(41) Harraz, F. A.; Faisal, M.; Jalalah, M.; Almadiy, A. A.; Al-Sayari, S. A.; Al-Assiri, M. S. Conducting Polythiophene/α-Fe_2O_3 Nanocomposite for Efficient Methanol Electrochemical Sensor. *Appl. Surf. Sci.* **2020**, *508*, 145226.
(42) Hosseinpour, M.; Fatemi, S.; Ahmadi, S. J.; Morimoto, M.; Akizuki, M.; Oshima, Y.; Fumoto, E. The Synergetic Effect between Supercritical Water and Redox Properties of Iron Oxide Nanoparticles during in-situ Catalytic Upgrading of Heavy Oil with Formic Acid. Isotopic Study. *Appl. Catal., B* **2018**, *230*, 91−101.
(43) Vostrikov, A. A.; Fedyaeva, O. N.; Shishkin, A. V.; Sokol, M. Y.; Zaikovskii, A. V. Synthesis of Fe_xO_y Nanoparticles during Iron Oxidation by Supercritical Water. *Tech. Phys. Lett.* **2012**, *38*, 955−958.
(44) Pereira, M. C.; Oliveira, L. C. A.; Murad, E. Iron Oxide Catalysts: Fenton and Fenton-like Reactions − a Review. *Clay Miner.* **2012**, *47*, 285−302.
(45) Ding, Z.-Y.; Aki, S. N. V. K.; Abraham, M. A. Catalytic Supercritical Water Oxidation: An Approach for Complete Destruction of Aromatic Compounds. *Innovations in Supercritical Fluids*; ACS Symp. Series; ACS: Washington, 1995; pp 232−245.
(46) Aki, S. N. V. K.; Ding, Z.-Y.; Abraham, M. A. Catalytic Supercritical Water Oxidation: Stability of Cr_2O_3 Catalyst. *AIChE J.* **1996**, *42*, 1995−2004.
(47) O'Brein, C. B.; Jenness, G. B.; Dong, H.; Vlachos, D. G.; Lee, I. C. Deactivation of Pt/Al_2O_3 during Propane Oxidation at Low Temperatures: Kinetic Regimes and Platinum Oxide Formation. *J. Catal.* **2016**, *337*, 122−132.
(48) Vostrikov, A. A.; Fedyaeva, O. N.; Shishkin, A. V.; Tretyakov, D. S.; Sokol, M. Y. Features of Low-Temperature Oxidation of Hydrogen in the Medium of Nitrogen, Carbon Dioxide, and Water Vapor at Elevated Pressure. *Int. J. Hydrogen Energy* **2018**, *43*, 10469−10480.
(49) Kritzer, P.; Boukis, N.; Dinjus, E. Corrosion of Alloy 625 in High-Temperature, High-Pressure Sulfate Solutions. *Corrosion* **1998**, *54*, 689−699.
(50) Fedyaeva, O. N.; Vostrikov, A. A.; Shishkin, A. V.; Sokol, M. Y.; Borisova, L. S.; Kashirtsev, V. A. Conversion of Brown Coal in Sub- and Supercritical Water at Cyclic Pressurization and Depressurization. *Russ. J. Phys. Chem. B* **2012**, *6*, 793−803.
(51) Powder Diffraction File, PDF-4+; Release 2012.

https://doi.org/10.1021/acsomega.1c00926
ACS Omega 2021, 6, 13134−13143